

## ACTIVE DISTURBANCE REJECTION CONTROL AND MODEL-FREE CONTROL TUNED VIA FICTITIOUS REFERENCE ITERATIVE TUNING

Raul-Cristian Roman<sup>1</sup>, Radu-Emil Precup<sup>1,2</sup>, Emil M. Petriu<sup>3</sup>

<sup>1</sup>Politehnica University of Timisoara,

Department of Automation and Applied Informatics, Timisoara, Romania

<sup>2</sup>Romanian Academy – Timisoara Branch,

Center for Fundamental and Advanced Technical Research, Timisoara, Romania


<sup>3</sup>University of Ottawa,


School of Electrical Engineering and Computer Science, Ottawa, Canada


ORCID iDs: Raul-Cristian Roman

Radu-Emil Precup

Emil M. Petriu

 <https://orcid.org/0000-0003-2551-7842>

 <https://orcid.org/0000-0002-2060-7403>

 <https://orcid.org/0009-0002-0548-8976>

**Abstract.** *This paper presents a comparative analysis of two data-driven algorithm combinations: the first-order Active Disturbance Rejection Control-Fictitious Reference Iterative Tuning (ADRC-FRIT) and the first-order Model-Free Control-Fictitious Reference Iterative Tuning (MFC-FRIT). The objective of both data-driven combinations is to ascertain the tunable parameters through the resolution of an optimization problem and to streamline the heuristic procedures involved. The data-driven algorithms are empirically validated through experimental trials utilizing the 3D laboratory equipment in which the x-, y-, and z-axes are controlled.*

**Key words:** *Active Disturbance Rejection Control, Model-Free Control, Fictitious Reference Iterative Control, 3D Crane*

### 1. INTRODUCTION

In recent years, the utilization of data-driven algorithms [1] in the control domain has seen a gradual increase. Within contemporary control systems, data-driven algorithms assume an increasingly pivotal role by using empirical data to design controllers with minimal reliance on explicit mathematical models, which is important in coping with

---

Received: May 20, 2025 / Accepted July 03, 2025

**Corresponding author:** Radu-Emil Precup

Politehnica University of Timisoara, Department of Automation and Applied Informatics, Bd. V. Parvan 2, 300223 Timisoara, Romania

Romanian Academy – Timisoara Branch, Center for Fundamental and Advanced Technical Research, Bd. Mihai Viteazu 24, 300223 Timisoara, Romania

E-mail: [radu.precup@upt.ro](mailto:radu.precup@upt.ro)

complex processing including active those involved in active structures [2]. Rather than designing precise system equations, these methodologies derive patterns and dynamics directly from input-output (I/O) data, thereby facilitating adaptation to intricate or uncertain environments. This method is particularly advantageous in contexts where traditional modeling proves impractical due to nonlinearities, noise, or high dimensionality. By seamlessly integrating tools from machine learning and optimization, data-driven control delivers flexible and robust solutions tailored to real-world applications, including robotics, energy systems, and autonomous vehicles. According to the authors, Active Disturbance Rejection Control (ADRC) [1,3,4], Model-Free Control (MFC) [1,5,6], Model-Free Adaptive Control [1,7], Virtual Reference Feedback Tuning [1,8], Iterative Feedback Tuning [1,9], Fictitious Reference Iterative Tuning (FRIT) [1,10], or Iterative Learning Control [11,12] are among the most frequently utilized data-driven algorithms.

ADRC is a feedback control strategy designed to handle uncertainties and external disturbances without relying on an accurate mathematical model of the process. At its core, ADRC augments the system's state with an estimated total disturbance, which encompasses both unknown dynamics and external inputs. This estimate is updated in real time by an observer and then actively canceled in the control law, resulting in improved robustness and disturbance rejection. Usually, due to its simplicity, the Extended State Observer (ESO) is preferred. Thanks to its model-agnostic design and straightforward tuning rules, ADRC has been successfully applied in fields ranging from robotics to process industries, where precise modeling proves challenging. Due to its model-independent framework and straightforward tuning guidelines, ADRC has been proficiently utilized across various domains. In the realm of tower crane systems, as indicated in [3], two configurations of ADRC integrated with the fuzzy logic technique are proposed, ensuring control loop stability as per fuzzy control system stability, with ADRC parameters determined through the metaheuristic Grey Wolf Optimizer. In [13], the second-order ADRC is combined with the sliding mode technique to enhance control loop performance, proposing ADRC stability while optimal controller parameters are ascertained via the metaheuristic slime mould algorithm (SMA) with validation on tower crane systems. According to [14], first-order ADRC is mixed with the FRIT to identify optimal tunable parameters using the metaheuristic African Vultures Optimization Algorithm (AVOA), accompanied by a proposed stability mechanism for ADRC, also validated on tower crane systems. For 3D crane systems in [15], comparisons are drawn between the first and second orders of ADRC algorithms. Direct Current (DC)-DC buck converters in [16] feature a general error-based ADRC with a stability mechanism founded on singular perturbation theory. In permanent magnet synchronous motors, as discussed in [17], a cascaded filter proportional-integral-derivative (PID) paradigm is employed for error-based ADRC, with system robustness characterized in terms of stability margins. In piezo-actuated beams, as described in [18], ADRC is utilized to estimate and compensate for total disturbances, with design based on the governing equation. For gimbal mechanisms, [19] proposes a first-order ADRC algorithm alongside a stability mechanism. The application of ADRC to rotary DC motors, as stated in [20], involves the use of an anti-windup strategy and Hurwitz polynomials. Across all these systems, the precise modeling remains a considerable challenge.

MFC, often associated with the concept of intelligent PID controllers, presents a viable alternative to traditional model-based control methodologies. Instead of relying on a detailed mathematical representation of the system, MFC builds on simplified local models based on real-time data. This approach allows the controller based on MFC to adapt to

system dynamics and external disturbances in the absence of preliminary identification procedures, making it especially valuable for complex or poorly understood processes. In recent years, MFC has been rigorously improved and validated across various demanding applications, from robotics to process industries, demonstrating its adaptability and efficacy in practical environments. In [5], the discrete-time MFC algorithm is employed, wherein the parameters of iPID controllers are optimally determined utilizing FRIT via the metaheuristic AVOA, subsequently validated through experimental trials on tower crane systems. In [21], the MFC is implemented in advanced processes, including the Quanser AERO. In [22], the MFC is validated across various scenarios on Wendling's model. In [23], MFC is experimentally applied to cloud and high-performance computing systems. In [24], MFC is utilized to manage processes involving shape memory alloys, specifically controlling a shape memory alloy spring-based actuator initially. In [25], the application of MFC, time-delay estimation MFC, and backstepping-based MFC is demonstrated in coupled mechatronic systems for controlling 2-DOF and 3-DOF robotic manipulators. In [26], MFC, in combination with Flatness-Based control, is employed for the management of unmanned surface vehicles. In [27], MFC is applied to the control of a prosthetic hand. In [28], MFC, coupled with a fuzzy technique, is utilized to control a twin rotor aerodynamic system. In all these applications, MFC proves to be highly beneficial due to the complexity and the challenge in determining precise mathematical models for these processes.

FRIT constitutes a data-driven iterative technique devised for the optimization of controllers, obviating the necessity for an explicit process model. The principal concept involves constructing a reference signal, designated as the fictitious reference, which, if pursued by the system, would produce an identical measured output. Through the iterative minimization of the error between the actual and desired behaviors, FRIT facilitates the direct adjustment of controller parameters utilizing solely experimental data, rendering it particularly suitable for systems where modeling is challenging or unreliable. Analogous to ADRC and MFC, FRIT has been substantiated across a diverse array of applications, encompassing robotics and process industries, thereby exhibiting its versatility and effectiveness within practical settings. In [29], an enhancement of FRIT through pseudo-linearization has been implemented on asymmetric Bouc-Wen systems. According to [30], FRIT is applied to the control of hydraulic systems and necessitates an offline database for the storage of historical process data. The study in [31] demonstrates the utilization of FRIT to calibrate the parameters of a fractional- and integer-order PID controller relevant to a benchmark problem encompassing both scenarios with and without time delay, specifically within a flexible transmission model. In [32], FRIT was employed to manage the cart position within a pendulum cart system. As observed in [33], FRIT is leveraged for the design of controller parameters in applications concerning a switched reluctance generator, ball screw positioning, two-mass resonance, and switched reluctance motor systems. Across these applications, FRIT effectively manages the feedback loop even when confronted with nonlinear processes.

The present paper seeks to build upon and synthesize the authors' prior work involving the integration of ADRC and MFC with FRIT. Initially, as indicated in [5], the discrete-time variant of the first-order MFC, incorporating a PID component, was integrated with FRIT, with the optimal controller parameters being computed via AVOA. Subsequently, [34] describes the blending of the continuous-time variant of the first-order MFC with a PI component with FRIT, with tuning via SMA for optimal parameters. Furthermore, in [35], a discrete-time, second-order version of the MFC algorithm with a P component is combined with FRIT, with optimal parameter settings adjusted using SMA. Additionally, [14] details the integration of the

first-order continuous-time ADRC with FRIT, where parameters were optimized utilizing the Gauss-Newton algorithm. Each of these algorithm integrations underwent experimental validation using tower crane systems. Accordingly, in the current paper, the authors integrate the continuous-time first-order MFC with a P component and the continuous-time first-order ADRC algorithms with FRIT, resulting in the ADRC-FRIT and MFC-FRIT algorithms. Both algorithms comprise one user-selected parameter and one tunable parameter whose optimal values will be ascertained through FRIT using the Newton–Raphson method. Stability mechanisms have been proposed for both ADRC and MFC algorithms, and stability is implicitly guaranteed for the ADRC-FRIT and MFC-FRIT algorithms. The efficacy of these algorithms is demonstrated through experiments performed using the 3D crane laboratory device [36], involving the control of the x-, y-, and z-axes. Metaheuristic algorithms such as AVOA and SMA, employed in solving optimization problems for the algorithms listed below, operate on the same principles as the metaheuristic BASO or ASO as detailed in [37]. Although the exact identification of the 3D crane system constitutes a labor-intensive endeavor, it can be achieved, for instance, through the application of dimension reduction via unsupervised learning [38].

The ensuing sections of this manuscript are systematically arranged as follows: Section 2 provides a comprehensive elucidation of the ADRC-FRIT and MFC-FRIT algorithms. Section 3 delivers a succinct description of the 3D crane. Section 4 presents a detailed exposition of the experimental results in conjunction with a critical analysis. Section 5 underscores the conclusions.

## 2. THE DATA-DRIVEN ALGORITHMS MIX

### 2.1. The FRIT Algorithms

The integration of continuous-time first-order ADRC and MFC with FRIT is advocated to ascertain the optimal parameters of the ADRC and MFC algorithms and to enhance the overall efficacy of the control system architecture. To achieve this objective, it is requisite to conduct an initial closed-loop experiment of the control system incorporating the ADRC algorithm. ADRC-FRIT and MFC-FRIT utilize the I/O data to resolve the optimization problem via the Newton–Raphson method

$$\mathbf{K}^* = \arg \min_{\mathbf{K}} J_{\mathbf{K}}(\mathbf{K}), J_{\mathbf{K}}(\mathbf{K}) = \frac{1}{T_H} \int_0^{T_H} [y_0(t, \mathbf{K}^{(0)}) - \tilde{y}_{\mathbf{K}}(t, \mathbf{K})]^2 dt, \quad (1)$$

where, in this context,  $\mathbf{K}^*$  denotes the optimal parameter either of the ADRC-FRIT or the MFC-FRIT algorithm as it pertains to  $\mathbf{K}$ , depending on the practitioner's choice. The initial parameter of these algorithms is represented by  $\mathbf{K}^{(0)}$ , with the superscript (0) satisfying its initial value. The cost function associated with the ADRC-FRIT or MFC-FRIT algorithm is denoted by  $J_{\mathbf{K}}$ . Notation  $T_H$  is used to specify the duration of the experimental timeframe. Furthermore,  $y_0(t, \mathbf{K}^{(0)})$  retains the output data obtained post the initial experiment. The fictitious reference model output  $\tilde{y}_{\mathbf{K}}(t, \mathbf{K})$  is determined through offline computation, given the understanding that [10,14,15,34,35]

$$\tilde{y}_{\mathbf{K}}(t, \mathbf{K}) = L^{-1} \{M(s) \tilde{r}(s, \mathbf{K})\}, \quad (2)$$

where the notation  $L^{-1}$  is utilized to represent the inverse Laplace transform. The reference model transfer function, denoted as  $M(s)$ , is determined by the designer to yield an output response that meets the performance specifications of the control system, and  $\tilde{r}(t, K)$  is the fictitious reference input, also referred to as the virtual set-point

$$\tilde{r}(t, K) = y_0(t, K^{(0)}) + L^{-1}\{u_0(s, K^{(0)})/C(s, K)\}, \quad (3)$$

$\tilde{r}(t, K)$  constitutes a modified version of the fictitious reference input as presented in [9] for continuous-time systems and corresponds to the improved virtual set-point for continuous-time systems outlined in [14] and [34], and for discrete-time systems in [6] and [35]. The term  $u_0(s, K^{(0)})$  denotes the input data, which is obtained using the Laplace transform and gathered from the initial closed-loop experiment, while  $C(s, K^{(0)})$  represents the transfer function of the proportional component within the ADRC or MFC algorithm [10,14,15,34,35]

$$C(s, K^{(0)}) = K. \quad (4)$$

To determine the value of gain  $K$  using the Newton-Raphson method [39] by computing the first and the second derivative of  $J_K(K)$ , i.e.,  $\partial J_K/\partial(K^{(i)})$  and  $\partial^2 J_K/\partial(K^{(i)})^2$ , and the solution is updated knowing that

$$K^{(i+1)} = K^{(i)} - \left( \frac{\partial^2 J_K}{(\partial K^{(i)})^2} \right)^{-1} \frac{\partial^2 J_K}{\partial K^{(i)}}, \quad (5)$$

where  $i$  is the index of the current iteration,  $J_K$  and  $J''_K$  are the first and the second derivative of  $J_K(K)$ .

As indicated by [10], the ADRC-FRIT algorithm identifies the I/O data-pair  $(u_0(t, K^{(0)}), y_0(t, K^{(0)}))$  as non-trivial, thereby [10,14,15,34,35]

$$\lim_{K \rightarrow K^*} \int_0^{T_H} (y(t, K) - \tilde{y}(t, K))^2 dt = \int_0^{T_H} \lim_{K \rightarrow K^*} \tilde{e}^2(t, K) dt. \quad (6)$$

## 2.2. The ADRC-FRIT Algorithms

The ADRC algorithm is designed for a continuous-time low-pass filter process

$$T \cdot \dot{y}(t) + y(t) = K \cdot u(t), \quad (7)$$

where  $t$  is the time variable,  $K$  is a member of the real numbers set  $R$ , represents the process gain, and  $T$ , also within  $R$ , signifies the process's time constant. The algorithm's capacity to operate with  $T$  values less than zero enables it to manage unstable processes effectively. Here,  $u(t)$ , a real-valued function, denotes the control input, while  $y(t)$ , also a real-valued function, indicates the controlled output. The revised process model is derived by incorporating the expression  $b = b_0 + \Delta b$ , where  $b_0$  serves as an estimator of the value of  $b \in R$ , and  $\Delta b$  accounts for the parametric uncertainty or variation in the gain parameter  $K$  of the system [13–15]

$$\dot{y}(t) = -(1/T)y(t) + (1/T)\delta(t) + (\Delta b + b_0)u(t). \quad (8)$$

In (8), the effect of the disturbance  $\delta(t)$  is evident, as the ADRC algorithm mitigates disturbance influences via an ESO, specifically a Luenberger observer. Conversely, in (7),

this disturbance is excluded to maintain a simplified representation of the nominal system model. The term that gathers all the unknowns of the process is the generalized disturbance term of the ADRC algorithm is

$$f(t) = -(1/T)y(t) + (1/T)\delta(t) + \Delta b \cdot u(t), \quad (9)$$

where function  $f(t)$  within R is contingent upon the known output  $y(t)$ , in contrast with the unidentified disturbances  $\delta(t)$  and the modeling error  $\Delta b$ , both of which affect the dynamics of the system. Within the context of the ESO in ADRC,  $y(t)$  is not directly observable and is instead approximated, thus included in  $f(t)$  together with the unknown disturbances  $\delta(t)$  and the modeling error  $\Delta b$ . Upon integrating the disturbance term from (8) into the first-order low-pass filter denoted as (7), the resulting process model transforms into a perturbed integrator [13–15]

$$\dot{y}(t) = f(t) + b_0 u(t). \quad (10)$$

Employing the notations  $z_1(t) = y(t)$  and  $z_2(t) = f(t)$  within expression (10), the state-space representation of the perturbed integrator model is

$$\begin{aligned} \begin{pmatrix} \dot{z}_1(t) \\ \dot{z}_2(t) \end{pmatrix} &= \begin{pmatrix} 0 & 1 \\ 0 & 0 \end{pmatrix} \mathbf{z}(t) + \begin{pmatrix} b_0 \\ 0 \end{pmatrix} u(t) + \begin{pmatrix} 0 \\ 1 \end{pmatrix} \dot{f}(t), \\ y(t) &= (1 \ 0) \mathbf{z}(t), \end{aligned} \quad (11)$$

where  $\mathbf{z}(t) = [z_1(t) \ z_2(t)]^T$ , with  $T$  representing matrix transposition, the third term in the right-hand side of (11) can be deemed negligible since the ESO, as introduced later in the discourse, can estimate and compensate for disturbances. The ADRC algorithm does not necessitate explicit disturbance modeling, as the observer performs real-time estimation and mitigation of disturbances. Consequently, the system can concentrate on its primary dynamics while the ESO addresses disturbances. Within the context of the ESO is employed to estimate the output of the system rather than the disturbance itself. This arises because, in the framework of ADRC, the observer is designed to estimate the system output directly. At the same time, the disturbance is inferred indirectly as a component of the total disturbance. This is achieved by analyzing the discrepancy between the observed output and the estimated output  $y(t) = \hat{z}_1(t)$ . Subsequently, upon substituting  $\hat{z}_1(t)$  with  $\hat{y}_1(t)$ , the model for the ESO is adjusted accordingly [13–15]

$$\begin{aligned} \underbrace{\begin{pmatrix} \dot{\hat{z}}_1(t) \\ \dot{\hat{z}}_2(t) \end{pmatrix}}_{\hat{\dot{\mathbf{z}}}(t)} &= \underbrace{\begin{pmatrix} -l_1 & 1 \\ -l_2 & 0 \end{pmatrix}}_{\mathbf{A}-\mathbf{LC}} \hat{\mathbf{z}}(t) + \underbrace{\begin{pmatrix} b_0 \\ 0 \end{pmatrix}}_{\mathbf{B}} u(t) + \underbrace{\begin{pmatrix} l_1 \\ l_2 \end{pmatrix}}_{\mathbf{L}} y(t), \\ \hat{y}(t) &= \underbrace{(1 \ 0)}_{\mathbf{C}} \hat{\mathbf{z}}(t), \end{aligned} \quad (12)$$

where the ESO gain matrices are  $\mathbf{A} \in \mathbb{R}^{2 \times 2}$ ,  $\mathbf{B} \in \mathbb{R}^{2 \times 1}$ , and  $\mathbf{C} \in \mathbb{R}^{1 \times 2}$ , while  $\mathbf{L} = [l_1 \ l_2]^T$  exerts an influence on the spectrum of matrix  $(\mathbf{A}-\mathbf{LC})$ , and  $\hat{\mathbf{z}}(t)$  is the estimate of  $\mathbf{z}(t)$ . The eigenvalues of the matrix  $(\mathbf{A}-\mathbf{LC})$  are required to reside in the left half-plane because their positions influence the behavior of the control system. Within this context, the feasible domain is denoted as  $D_L$ . Here,  $y(t)$  represents the controlled output obtained from an initial open-loop experiment, and  $\hat{z}_1(t) = y(t)$ , which is the primary output produced by the

observer estimating  $y(t)$ . The initial open-loop experiment is executed under a dynamic regime that is congruent with the closed-loop control system's operating conditions. Furthermore, the input signal applied to the open-loop experiment must be rich in frequency content. The characteristic polynomial associated with the ESO's dynamic model is [14]

$$\mu(s) = s^2 + l_1 s + l_2. \quad (13)$$

The stability of the ESO is guaranteed by enforcing the characteristic polynomial in (13) to satisfy Hurwitz conditions, thereby resulting in the establishment of constraints for determining the elements of  $\mathbf{L}$

$$D_{\mathbf{L}} = \{[l_1 \ l_2]^T \in \mathbf{R}^2 \mid l_1 > 0, l_2 > 0\}. \quad (14)$$

The control strategy formulated for the ADRC algorithm is

$$u(t) = \frac{1}{b_0} \left( \underbrace{K(r(t) - \hat{z}_1(t))}_{\hat{e}(t)} - \hat{z}_2(t) \right) = \frac{1}{b_0} (K\hat{e}(t) - \hat{z}_2(t)), \quad (15)$$

where  $\hat{e}(t)$  represents the estimated control error, and  $e(t) = r(t) - z_1(t) = r(t) - y(t)$  denotes the control error,  $r(t)$  is the reference input (set-point), and  $K$  is the ADRC's gain.

The stability of the control system with the ADRC algorithm and ESO, denoted as  $\mathbf{K}_{\text{ADRC}} = [K \ l_1 \ l_2]^T$ , is ensured by Theorem 1 [14] with the proof given in [40].

**Theorem 1.** Taking into account the disturbed integrator model (10) alongside the disturbance term (9), in conjunction with the ESO dynamic model (12), the ADRC control system employing the control law (15) is stable if and only if

$$\begin{aligned} \mathbf{K}_{\text{ADRC}} \in D_{\text{ADRC}} \subset \mathbf{R}^3, D_{\text{ADRC}} = \{& (K \ l_1 \ l_2)^T \mid l_1 > 0, l_2 > 0, K + l_1 + \frac{1}{T} > 0, \\ & \frac{1}{T}(K + l_1) + (Kl_1 + l_2)b/b_0 > 0, Kb/b_0 > 0, \\ & \frac{1}{T^2}(K + l_1) + \frac{1}{T}(Kl_1 + l_2)b/b_0 + \frac{1}{T}(K + l_1)^2 + (K^2l_1 + Kl_1^2 + l_1l_2)b/b_0 > 0, \\ & Kl_2b/b_0[\frac{1}{T^2}(K + l_1) + \frac{1}{T}(Kl_1 + l_2)b/b_0 + \frac{1}{T}(K + l_1)^2 + (K^2l_1 + Kl_1^2 + l_1l_2)b/b_0] > 0\}. \end{aligned} \quad (16)$$

In designing the ADRC-FRIT algorithm, theoretical considerations from the current subsection, as well as those of FRIT in Subsection 2.1, are meticulously incorporated.

In the context of ADRC-FRIT, for the initial experiment, the practitioner should set a value of  $K$ , and therefore, the domain (16) will be reduced to  $D_{\mathbf{L}}(K) = \{[l_1 \ l_2]^T \in \mathbf{R}^2 \mid [K \ l_1 \ l_2]^T \in D_{\text{ADRC}}\}$ . Controller tuning heuristics can be minimized by setting matrix  $\mathbf{L} = [l_1 \ l_2]^T$  as the solution  $\mathbf{L}^* = [l_1^* \ l_2^*]^T$  to the optimization problem [14]

$$\mathbf{L}^* = \arg \min_{\mathbf{L} \in D_{\mathbf{L}}(K_1)} J_{\mathbf{L}}(\mathbf{L}), \quad J_{\mathbf{L}}(\mathbf{L}) = \frac{1}{T_H} \int_0^{T_H} (e(t, \mathbf{L}))^2 dt. \quad (17)$$

The subsequent implementation of ADRC-FRIT is realized by adhering to the steps outlined below:

*Step 1.1.* The designer defines the initial conditions of the open-loop experiment.

*Step 1.2.* The designer must assign a value other than zero to the estimated coefficient of the control input, denoted as  $b_0$ . Additionally, the designer should establish an appropriate value for  $K$ , which represents the gain of the ADRC algorithm (or controller gain), specifically  $K^{(0)}$ , as the initial parameter of the ADRC-FRIT algorithm.

*Step 1.3.* In the dynamic regime and context tailored to the optimization problem given in (17), constrained by (16), the optimization problem stated in equation (17) is solved using the Newton-Raphson method to determine the optimal ESO parameter vector,  $\mathbf{L}^* = [l_1^* \ l_2^*]^T$ .

*Step 1.4.* The ADRC algorithm is validated in a closed-loop control experiment. This coincides with the ADRC-FRIT initial experiment.

*Step 1.5.* A reference model  $M(s)$  is set to ensure the output meets the control system's performance criteria.

*Step 1.6.* To determine the fictitious reference  $\tilde{r}(t, K)$  accordance with (3), the I/O data pair  $(u_0(t, \mathbf{K}^{(0)}), y_0(t, \mathbf{K}^{(0)}))$  is acquired. Next, the fictitious reference model output  $\hat{y}_K(t, K)$  is derived in accordance with (2).

*Step 1.7.* To calculate the optimal parameter  $K^*$  for the ADRC-FRIT algorithm, the control error from the previous experiment is used as the benchmark input in the gradient experiment. This is carried out with (5), applying the Newton-Raphson method to solve the optimization challenge outlined in equation (1).

*Step 1.8.* An experiment with the control system's closed-loop structure, employing the ADRC algorithm with parameter  $K^*$  optimally determined via FRIT, is conducted.

The procedures outlined in Steps 2.6-2.8 are repeated numerous times to improve the overall efficacy of the control system. The input/output data collected upon the completion of Step 2.8 is subsequently employed in Step 2.6 for a new iteration.

### 2.3. The MFC-FRIT Algorithms

The MFC algorithms incorporating a P component, commonly identified in contemporary research as the iP controller, are designed based on the first-order local process model similar to (7) [1,5,6,21–23,34,35]

$$\dot{y}(t) = F(t) + \alpha u(t), \quad (18)$$

where  $F(t)$  represents unmodeled dynamics and disturbances,  $u(t)$  and  $y(t)$  have the same significance as in the ADRC case, while  $\alpha > 0$  for balancing  $\dot{y}(t)$  and  $\alpha u(t)$ .

The MFC algorithm is predicated upon the subsequent specific control law

$$u(t) = -[\hat{F}(t) - \dot{r}(t) + Ke(t)] / \alpha, \quad (19)$$

where, in the context of the MFC algorithm,  $K$  represents the proportional constant, specifically the gain associated with the P component of the MFC algorithm.  $\hat{F}(t)$  denotes the estimation of  $F(t)$  derived from the I/O data of  $u(t)$  and  $y(t)$ . Furthermore,  $r(t)$  holds an equivalent significance as observed within the framework of the ADRC algorithm, and its first-order derivative is estimated through the utilization of a derivative plus low-pass filter, characterized by [1,5,6,21–23,34,35]

$$H_F(s) = s / (1 + T_F s), \quad (20)$$



where the time constant of the first-order derivative filter, denoted as  $T_F$ , ought to be selected by the practitioner as a small positive value to ensure precise estimation of derivatives. The signals processed through  $H_F(s)$  in (20), represented as  $\dot{r}(t)$  and  $\dot{y}(t)$ , will henceforth be referred to as  $\hat{r}(t)$  and  $\hat{y}(t)$ , respectively. Additionally,  $e(t)$  maintains the same definition as it does within the framework of the ADRC algorithm. The derivation of  $\hat{F}(t)$  is based on the first-order local process model equation given in (18), which is transformed as follows:

$$\hat{F}(t) = \hat{y}(t) - \alpha u(t). \quad (21)$$

The stability of a control system utilizing the MFC algorithm is guaranteed if the characteristic polynomial, obtained by substituting the control law from equation (19) into the local process model delineated in equation (18)

$$\dot{e}(t) - K e(t) = 0, \quad (22)$$

exhibits roots situated within the left half-plane; therefore,  $K < 0$ , and the estimation error denotes  $\delta(t) = F(t) - \hat{F}(t)$  is assumed to be zero, and  $\dot{e}(t) = \dot{r}(t) - \dot{y}(t)$ . The stability of the control system with the MFC algorithm  $K_{MFC} = K$  is ensured by Theorem 2, with the proof taken from [41].

**Theorem 2.** Considering the first-order local process model as detailed in (18) alongside the control law delineated in (19), as well as the unmodeled dynamics and disturbances specified in (21), assuming  $\delta(t)$  equals zero, and evaluating the characteristic polynomial of the error dynamics presented in (22), the stability of the control system is ensured if the roots of (22) reside in the left half-plane. Therefore, the MFC control system employing the control law (19) is stable if and only if

$$K_{MFC} \in D_{MFC} \subset \mathbf{R}, D_{MFC} = \{K \mid K < 0\}. \quad (23)$$

The subsequent implementation of MFC-FRIT is realized by crossing to the outlined steps:

*Step 2.1.* The designer defines the initial conditions of the closed-loop experiment.

*Step 2.2.* The designer must assign a value other than zero to  $\alpha$ . Additionally, the designer should establish an appropriate value for  $K$ , which represents the gain of the MFC algorithm (or controller gain), specifically  $K^{(0)}$ , as the initial parameter of the MFC-FRIT algorithm.

*Step 2.3.* The designer should establish the derivative plus low-pass filter in (20) by setting a small positive value for  $T_F$ .

*Step 2.4.* The MFC algorithm is validated in a closed-loop control experiment. This coincides with the MFC-FRIT initial experiment.

*Steps 2.5 to 2.8* are identical to steps 1.5 to 1.8, as is the case with the ADRC algorithm, and are applied for the case of the MFC algorithm. Therefore, the procedures outlined in Steps 2.6-2.8 are repeated numerous times to improve the overall efficacy of the control system. The input/output data collected upon the completion of Step 2.8 is subsequently employed in Step 2.6 for a new iteration.

The block diagrams of the ADRC-FRIT and MFC-FRIT algorithms are depicted in Fig. 1 a) and b), respectively.

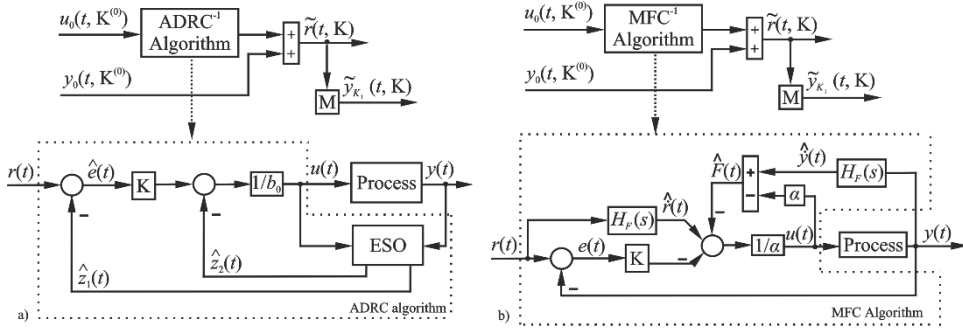


**Fig. 1** The block diagrams of the ADRC-FRIT in a) and MFC-FRIT in b).

### 3. THE 3D CRANE

The validation of the continuous-time first-order ADRC-FRIT and MFC-FRIT is performed with experimental setups involving the 3D crane laboratory equipment, where control is applied to the x-, y-, and z-axes. Details of the laboratory configuration and the mathematical model, highlighting the complex dynamics due to nonlinearity, are recorded in [36].

The 3D crane is operated using three control inputs  $u_i \in [-1, 1]$ ,  $i \in \{1, 2, 3\}$ , which modulate the duty cycles of pulse width to control the DC motors, thereby actuating the x-, y-, and z-axes. Specifically,  $x_1(m) = y_1(m)$  denotes the cart's position along the x-axis,  $x_3(m) = y_2(m)$  corresponds to its position along the y-axis, and  $x_9(m) = y_3(m)$  represents the payload's position along the z-axis.

### 4. THE SETUP AND RESULTS

To have a fair comparison of the ADRC-FRIT and MFC-FRIT algorithms, both are validated using experiments considering the same set-up, i.e., 70 s as time horizon, and the reference inputs (set-point) are  $r_i(t)$  obtained as the signals  $\tau_i(t)$  filtered through  $H_{r_i}(s)$ ,  $i \in \{1, 2, 3\}$ :

$$\begin{aligned} \tau_1(t) &= 0.15 \text{ if } t \in [0, 20], 0.1 \text{ if } t \in (20, 35], -0.05 \text{ if } t \in (35, 50], 0 \text{ if } t \in (50, 70], \\ \tau_2(t) &= 0 \text{ if } t \in [0, 5], 0.15 \text{ if } t \in (5, 25], -0.15 \text{ if } t \in (25, 40], 0 \text{ if } t \in (40, 70], \\ \tau_3(t) &= 0 \text{ if } t \in [0, 15], 0.1 \text{ if } t \in (15, 30], -0.05 \text{ if } t \in (30, 45], 0 \text{ if } t \in (45, 70], \end{aligned} \quad (24)$$

$$H_{r_1}(s) = 1/(1 + 0.2s), H_{r_2}(s) = 1/(1 + 0.21s), H_{r_3}(s) = 1/(1 + 0.3s). \quad (25)$$

The effectiveness of the data-driven algorithms shall be evaluated utilizing the forthcoming performance index:

$$J_{e,u}(K_\diamond) = \frac{1}{T_H} \int_0^{T_H} [e_1^2(t, K_{\diamond 1}) + e_2^2(t, K_{\diamond 2}) + e_3^2(t, K_{\diamond 3})] dt, \quad (26)$$

where the time horizon is  $T_H = 70$  s, the subscript  $\diamond$  represents one of the following: ADRC, ADRC-FRIT, MFC, MFC-FRIT, each of which corresponds to the data-driven algorithms

discussed within this paper. Additionally, the subscripts 1, 2, and 3 denote the parameters corresponding to the x-, y-, and z-axes, respectively.

According to Steps 1.1 to 1.4, the ADRC algorithms are designed by considering the open-loop experiment a signal rich in frequency content (Step 1.1). Next, the practitioner assigns the values of  $b_0 = 1$  and  $K$ , which will later be employed as  $K^{(0)}$  in the ADRC-FRIT (Step 1.2), obtaining  $K_{\text{ADRC1}} = 1.3432$ ,  $K_{\text{ADRC2}} = 1.3541$ , and  $K_{\text{ADRC3}} = 1.4135$ .

By solving the optimization problem in (17) in terms of (16) using the Newton-Raphson method, the optimal parameters of ESO are (Step 1.3)  $\mathbf{L}_1^* = [192.1 \ 9224.1]^T$ ,  $\mathbf{L}_2^* = [146.8 \ 5388.3]^T$ ,  $\mathbf{L}_3^* = [172.4 \ 7416.7]^T$ . The validation of the closed-loop ADRC algorithm coincides with the initial experiment of the ADRC-FRIT algorithm, considering the reference inputs (set-point) described above for the closed-loop experiments (Step 1.4). In the next phase, the designer sets the reference model  $M(s)$  chosen to meet the control system performance criteria, and in this case,  $M(s)$  is  $H_r(s)$  as given in (25) (Step 1.5). With the I/O data collected in Step 1.4, the fictitious reference  $\tilde{r}(t, K)$  and fictitious reference model output  $\tilde{y}_k(t, K)$  are computed in terms of (3) and (2) (Step 1.6). The optimal parameter  $K^*$  of the ADRC-FRIT algorithm is determined after ten iterations by solving (1) using the Newton-Raphson method and obtaining (Steps 1.7 and 1.8)  $K_{\text{ADRC-FRIT1}}^* = 5.8716$ ,  $K_{\text{ADRC-FRIT2}}^* = 4.8671$ ,  $K_{\text{ADRC-FRIT3}}^* = 3.3211$ .

According to Steps 2.1 to 2.4, the MFC algorithms are designed by considering the closed-loop experiment, with the same reference inputs as above (Step 2.1). Next, the practitioner assigns the values of  $\alpha = 1$  and  $K$ , later used as  $K^{(0)}$  in the MFC-FRIT algorithm (Step 2.2), obtaining  $K_{\text{MFC1}} = -22.9093$ ,  $K_{\text{MFC2}} = -21.0261$ , and  $K_{\text{MFC3}} = -29.0214$ . The designer establishes that  $T_F = 0.001$  for the low-pass filter in (20) (Step 2.3). The validation of the closed-loop MFC algorithm coincides with the initial experiment of the MFC-FRIT algorithm (Step 2.4). In the next phase, the designer uses the same reference model  $M(s)$  as in the ADRC-FRIT chosen to meet the control system performance (Step 2.5). With the I/O data collected in Step 2.4, the fictitious reference  $\tilde{r}(t, K)$  and fictitious reference model output  $\tilde{y}_k(t, K)$  are computed in terms of (3) and (2) (Step 2.6). The optimal parameter  $K^*$  of the MFC-FRIT algorithm is determined after ten iterations by solving (1) using the Newton-Raphson method and obtaining (Steps 2.7 and 2.8)  $K_{\text{MFC-FRIT1}}^* = -33.9101$ ,  $K_{\text{MFC-FRIT2}}^* = -31.0199$ ,  $K_{\text{MFC-FRIT3}}^* = -49.0200$ .

The outcomes of the real-time experiments are illustrated in Figs. 1-3 within the supplementary material in [42], as well as in Table 2. These outcomes represent the averages of ten distinct sets of real-time experiments conducted to mitigate random disturbances that may arise during an experiment. No additive disturbances were introduced in the real-time experiments. The experimental data distinctly indicate that ADRC and MFC exhibit equivalent performance in the initial experiment. Subsequent to determining the optimal parameters with FRIT, the experimental results derived from ADRC-FRIT and MFC-FRIT surpass those of the initial closed-loop experiments. Moreover, similar to the initial closed-loop experiment, ADRC-FRIT and MFC-FRIT perform equivalently. However, concerning the 3D crane equipment, MFC and MFC-FRIT demonstrate slightly superior performance. However, these conclusions might be different if combinations of data-driven control with model-based control including fuzzy control [4,12,28,43], [42], and sliding mode control [44,45].

**Table 1** The average and the variance of the performance index in (27)

	ADRC	ADRC-FRIT	MFC	MFC-FRIT
Average of $J_{e,u}$	$9.8043 \cdot 10^{-4}$	$3.5911 \cdot 10^{-4}$	$5.9425 \cdot 10^{-4}$	$3.3567 \cdot 10^{-4}$
Variance of $J_{e,u}$	$1.9881 \cdot 10^{-11}$	$2.0014 \cdot 10^{-11}$	$2.1015 \cdot 10^{-11}$	$1.9988 \cdot 10^{-11}$

## 5. CONCLUSIONS

This paper aims to conduct a comparative analysis of two data-driven integrations, specifically the first-order continuous-time ADRC-FRIT and MFC-FRIT algorithms, as validated through experimental testing on 3D crane laboratory equipment. The innovative aspects of this study include the integration of the first-order continuous-time ADRC and MFC with FRIT, the determination of optimal parameters for ADRC and MFC using FRIT by resolving the optimization problem in (1) via the Newton–Raphson method, and the validation of the first-order continuous-time ADRC, ADRC-FRIT, MFC, and MFC-FRIT algorithms on the 3D crane system.

Future research will concentrate on validating the proposed data-driven algorithms presented in this paper on other real-time devices, as well as on the integration and enhancement of data-driven algorithms such as ADRC, MFC, or FRIT.

**Acknowledgement:** *This work was supported by a grant of the Ministry of Research, Innovation and Digitization, CNCS/CCCDI - UEFISCDI, project number ERANET-ENUAC-e-MATS, within PNCDI IV, and the NSERC of Canada.*

## REFERENCES

1. Precup, R.-E., Roman, R.-C., Safaei, A., 2021, *Data-Driven Model-Free Controllers*, 1<sup>st</sup> Edition, CRC Press, Taylor & Francis, Boca Raton, FL, USA.
2. Milić, P., Marinković, D., Klinge, S., Čojbašić, Ž., 2023, *Reissner-Mindlin based isogeometric finite element formulation for piezoelectric active laminated shells*, Tehnički Vjesnik, 30(2), pp. 416-425.
3. Z. Gao, 2006, *Active disturbance rejection control: a paradigm shift in feedback control system design*, Proc. 2006 American Control Conference, Minneapolis, MN, USA, pp. 2399–2405.
4. Roman, R.-C., Precup, R.-E., Petriu, E. M., 2021, *Hybrid data-driven fuzzy active disturbance rejection control for tower crane systems*, European Journal of Control, 58, pp. 373-387.
5. Fliess, M., Join, C., 2013, *Model-free control*, International Journal of Control, 86(12), pp. 2228–2252.
6. Roman, R.-C., Precup, R.-E., Petriu, E. M., Muntyan, M., 2023, *Fictitious reference iterative tuning of discrete-time model-free control for tower crane systems*, Studies in Informatics and Control, 32(1), pp. 5-14.
7. Liu, S., Lin, G., Ji, H., Jin, S., Hou, Z., 2025, *A novel enhanced data-driven model-free adaptive control scheme for path tracking of autonomous vehicles*, IEEE Transactions on Intelligent Transportation Systems, 26(1), pp. 579-590.
8. Formentin, S., Campi, M. C., Carè, A., Savaresi, S. M., 2019, *Deterministic continuous-time virtual reference feedback tuning (VRFT) with application to PID design*, Systems & Control Letters, 127, pp. 25-34.
9. Hjalmarsson, H., 2002, *Iterative feedback tuning*, International Journal of Adaptive Control and Signal Processing, 16(5), pp. 373-395.
10. Soma, S., Kaneko, O., Fujii, 2004, *A new method of controller parameter tuning based on input-output data – Fictitious Reference Iterative Tuning (FRIT)*, IFAC Proceedings Volumes 37(12), pp. 798-794.
11. Bristow, D.A., Tharayil, M., Alleyne, A.G., 2006, *A survey of iterative learning control*, IEEE Control Systems Magazine, 26(3), pp. 96-114.
12. Precup, R.-E., Roman, R.-C., Hedrea, E.-L., Petriu, E. M., Bojan-Dragos, C.-A., Szedlak-Stinean, A.-I., 2024, *Metaheuristic-based tuning of proportional-derivative learning rules for proportional-integral fuzzy controllers in tower crane system payload position control*, Facta Universitatis-Series Mechanical Engineering, 22(4), pp. 567-582.

13. Roman, R.-C., Precup, R.-E., Petriu, E. M., Borlea, A.-I., 2024, *Hybrid data-driven active disturbance rejection sliding mode control with tower crane systems validation*, Romanian Journal of Information Science and Technology, 27(1), pp. 3-17.
14. Roman, R.-C., Precup, R.-E., Stebel, K., Madonski, R., 2025, *Active disturbance rejection control tuned by fictitious reference iterative tuning for tower crane systems*, Proc. 23<sup>rd</sup> European Control Conference (ECC), Thessaloniki, Greece, pp. 1-8.
15. Roman, R.-C., Precup, R.-E., Petriu, E. M., 2024, *Active disturbance rejection control for 3D crane systems*, Procedia Computer Science, 242, pp. 976-983.
16. Madonski, R., Shao, S., Zhang, H., Gao, Z., Yang, J., Li, S., 2019, *General error-based active disturbance rejection control for swift industrial implementations*, Control Engineering Practice, 84, pp. 218-229.
17. Cao, M., Yang, J., Li, S., Madonski, R., Xue, W., 2025, *Cascaded filter PID paradigm for error-based active disturbance rejection control: equivalence, design, and implementation guidelines*, IEEE Transactions on Industrial Electronics, doi: 10.1109/TIE.2025.3559950, pp. 1-11.
18. Sun, X. G., Chi, W. C., Wang, Y. Q., 2024, *Linear active disturbance rejection control algorithm for active vibration control of piezo-actuated beams: Theoretical and experimental studies*, Thin-Walled Structures, 199, paper 111782.
19. Ahi, B., Nobakhti, A., 2018, *Hardware implementation of an ADRC controller on a gimbal mechanism*, IEEE Transactions on Control Systems Technology, 26(6), pp. 2268-2275.
20. Ahi, B., Haeri, M., 2018, *Linear active disturbance rejection control from the practical aspects*, IEEE/ASME Transactions on Mechatronics, 23(6), pp. 2909-2919.
21. Fliess, M., Join, C., 2012, *An alternative to proportional-integral and proportional-integral-derivative regulators: Intelligent proportional-derivative regulators*, International Journal of Robust and Nonlinear Control, 32(18), pp. 9512-9524.
22. Join, C., Jovellar, D. B., Delaleau, E., Fliess, M., 2024, *Detection and suppression of epileptiform seizures via model-free control and derivatives in a noisy environment*, Proc. IEEE 12<sup>th</sup> International Conference on Systems and Control, Batna, Algeria, pp. 1-6.
23. Guilloteau, Q., Robu, B., Join, C., Fliess, M., Rutten, E., Richard, O., 2022, *Model-free control for resource harvesting in computing grids*, Proc. 2022 6<sup>th</sup> IEEE Conference on Control Technology and Applications, Trieste, Italy, pp. 1-7.
24. Gedouin, P.-A., Delaleau, E., Bourgeot, J.-M., Join, C., Chirani, S. A., Calloch, S., 2011, *Experimental comparison of classical PID and model-free control: Position control of a shape memory alloy active spring*, Control Engineering Practice, 19(5), pp. 433-441.
25. He, D., Wang, H., Tian, Y., Fliess, M., 2025, *MIMO ultra-local model-based adaptive enhanced model-free control using extremum-seeking for coupled mechatronic systems*, ISA Transactions, 157, pp. 233-247.
26. Degorre, L., Delaleau, E., Join, C., Fliess, M., 2025, *A novel approach to guidance and control of USVs combining flatness-based and model-free controllers*, Proc. 9<sup>th</sup> IFAC Symposium on System Structure and Control (SSSC 2025), Gif-sur-Yvette, France, pp. 1-6.
27. Precup, R.-E., Roman, R.-C., Teban, T.-A., Albu, A., Petriu, E. M., Pozna, C., 2020, *Model-free control of finger dynamics in prosthetic hand myoelectric-based control systems*, Studies in Informatics and Control, 29(4), pp. 399-410.
28. Roman, R.-C., Precup, R.-E., David, R.-C., 2018, *Second order intelligent proportional-integral fuzzy control of twin rotor aerodynamic systems*, Procedia Computer Science, 139, pp. 372-380.
29. Sekine, M., Tsuruhara, S., ITO, K., 2025, *Optimized design of a pseudo-linearization-based model predictive controller: Direct data-driven approach*, IET Control Theory & Applications, 19(1), pp. 1-17.
30. Li, Z., Hiraoka, K., Yamamoto, T., 2024, *Design and experimental evaluation of a data-driven PID controller using cerebellar memory*, IET Control Theory & Applications, 18(11), pp. 1371-1382.
31. Yonezawa, A., Yonezawa, H., Yahagi, D., Kajiwara, I., 2024, *Practical one-shot data-driven design of fractional-order PID controller: Fictitious reference signal approach*, ISA Transactions, 152, pp. 208-216.
32. Kaneko, O., Soma, S., Fujii, T., 2005, *A Fictitious Reference Iterative Tuning (FRIT) in the two-degree of freedom control scheme and its application to closed loop system identification*, IFAC Proceedings Volumes, 38(1), pp. 626-631.
33. Ikeda, H., Goto, K., Zhang, F., Kayashima, K., Hanamoto, T., 2018, *Application of fictitious reference iterative tuning to controller design for various machines*, Proc. 2018 International Power Electronics Conference, Niigata, Japan, pp. 1315-1321.
34. Roman, R.-C., Precup, R.-E., Petriu, E. M., Muntyan, M., Hedrea, E.-L., 2023, *Fictitious reference iterative tuning of intelligent proportional-integral controllers for tower crane systems*, Proc. 2023 31<sup>st</sup> Mediterranean Conference on Control and Automation, Limassol, Cyprus, pp. 740-746.
35. Roman, R.-C., Precup, R.-E., Hedrea, E.-L., 2023, *Intelligent proportional controller tuned by virtual reference feedback tuning and fictitious reference iterative tuning*, Procedia Computer Science 221, pp. 86-93.

36. Inteco, 2012, *3D Crane, User's Manual*, Inteco Ltd., Krakow, Poland.
37. Kilic, U., Sarac Essiz, E., Kaya Keles, M., 2023, *Binary anarchic society optimization for feature selection*, Romanian Journal of Information Science and Technology, 26(3-4), pp. 351-364.
38. Lu, Z.-L., Lok, U. H., 2024, *Dimension-reduced modeling for local volatility surface via unsupervised learning*, Romanian Journal of Information Science and Technology, 27(3-4), pp. 255-266.
39. Pho, K.-H., 2022, *Improvements of the Newton-Raphson method*, Journal of Computational and Applied Mathematics, 408, paper 114106.
40. Roman, R.-C., Precup, R.-E., Stebel, K., Madonski, R., 2024, *Supplementary material of the paper Raul-Cristian Roman, Radu-Emil Precup, Krzysztof Stebel, Rafal Madonski, Active Disturbance Rejection Control Tuned by Fictitious Reference Iterative Tuning for Tower Crane Systems*, the 23<sup>rd</sup> European Control Conference (ECC), [Online]. Available: [https://uptro29158-my.sharepoint.com/:f/g/personal/raul-cristian\\_roman\\_upt\\_ro/EljHGKk30Z1Alwd0rNNp8BTMpi742jM4v8s9MPgdBz2g?e=9rOXjd](https://uptro29158-my.sharepoint.com/:f/g/personal/raul-cristian_roman_upt_ro/EljHGKk30Z1Alwd0rNNp8BTMpi742jM4v8s9MPgdBz2g?e=9rOXjd) (last access: 31.10.2024).
41. Fliess, M., Join, C., 2014, *Stability margins and model-free control: A first look*, Proc. 2014 European Control Conference, Strasbourg, France, pp. 454-459.
42. Roman, R.-C., Precup, R.-E., Petriu, E. M., *Supplementary appendix of the paper Active Disturbance Rejection Control and Model-Free Control Tuned via Fictitious Reference Iterative Tuning*, [Online]. Available: [https://uptro29158-my.sharepoint.com/:f/g/personal/raul-cristian\\_roman\\_upt\\_ro/EidruGdukWlGtba5YbQ0lqgBqAno8M91gUXs8t1FrqW8lA?e=ygQXw4](https://uptro29158-my.sharepoint.com/:f/g/personal/raul-cristian_roman_upt_ro/EidruGdukWlGtba5YbQ0lqgBqAno8M91gUXs8t1FrqW8lA?e=ygQXw4) (last access 31.05.2025).
43. Čojbašić, Ž. M., Nikolić, V. D., Ćirić, I. T., Čojbašić, L. R., 2011, *Computationally intelligent modeling and control of fluidized bed combustion process*, Thermal Science, 15(2), pp. 321-338.
44. Borlea, A.-I., Precup, R.-E., Roman, R.-C., 2023, *Discrete-time model-based sliding mode controllers for tower crane systems*, Facta Universitatis-Series Mechanical Engineering, 21(1), pp. 1-20.
45. Guvenc, M. A., Bilgic, H. H., Mistikoglu S., 2023, *Identification of chatter vibrations and active vibration control by using the sliding mode controller on dry turning of titanium alloy (Ti6AL4V)*, Facta Universitatis-Series Mechanical Engineering, 21(2), pp. 307-322.